Electronic Supplementary Material (ESI) for Environmental Science: Nano.

Supporting information

Real-time assessment of the impacts of polystyrene and silver nanoparticles on hatching process and early-stage development of *Artemia* using a microfluidic platform

Preyojon Dey,[a] Terence M. Bradley [b] and Alicia Boymelgreen*[a]

a. Department of Mechanical and Materials Engineering, Florida International University, 10555 W Flagler St, Miami, FL, 33174, USA.

b. Department of Fisheries, Animal and Veterinary Science, University of Rhode Island, Kingston, RI 02881, USA.

* Corresponding author, E-mail: aboymelg@fiu.edu

Text S1. Nanoparticles characterization

After drop-casting nanoparticle (NP) suspension onto double-sided carbon tape on a glass coverslip, they were air-dried overnight before scanning electron microscopy (SEM) imaging (JEOL FS-100) was performed to characterize their morphology [Figure S1(A-B)]. Dynamic light scattering (DLS) (Nano ZS, Malvern instruments) was performed to assess the size and charge of the NPs and the aggregation behavior of the NPs in artificial saltwater (ASW). ASW was prepared by mixing sea salt (Fluval Sea, includes Ca, K, Mg, and Sr) with deionized water (DIW) (Barnstead Smart2Pure Water Purification System) and thoroughly mixed for even dissolved oxygen and salt distribution. The pH of the initial DIW solution was ~8. NPs were suspended in ASW with 25 parts per thousand (ppt) salinity using a vortex mixer (Vortex genie 2, Scientific Industries) to prepare NP suspension at 0.01, 0.1, 0.5, and 1 mg/L. NP suspension was incubated at 25°C for 24 h and NP's behavior at different concentrations was tested by DLS after 1 and 24 h, with triplicate experiments [Figure S1(C-D)]. Before testing, ASW was filtered (0.22 μm pore size) and mixed with varied NP concentrations. Additionally, after 24 h, photos were taken at the tube bottom to assess probable sedimentation [Figure S1(E)].

Text S2. *Artemia* cysts and hatching

Procured *Artemia* cysts were initially stored at 4°C. Before hatching experiments, they were adjusted to room temperature overnight. The cysts were hatched for 24 hours using a microfluidic platform comprising of a polydimethylsiloxane (PDMS) hatching chip (volume = ~563 μL) with a cylindrical enclosed chamber placed on a proportional–integral– derivative (PID) controlled heater for hatching at 25°C. In our previous study, we found that the hatching process of *Artemia* cysts was most successful (yielded the highest hatching rate) when the temperature and salinity of the ASW were set at 25°C and 25 ppt, respectively. Therefore, we have chosen to use these optimal

values for the present study (1). An oxygen sensor spot (OXSP5, Pyroscience) was placed in the chip, connected to an optical oxygen meter (FireSting®-O2, Pyroscience) which measures dissolved oxygen concentration in the hatching media at a rate of 1 Hz. For hatching experiments, cyst suspension in ASW or NP-spiked ASW chips were sealed to prevent air infiltration. At the beginning of the experiment, the dissolved oxygen concentration at 25°C temperature and 25 ppt salinity was observed to vary between 7.12-7.22 mg/L, irrespective of NP condition. A digital microscope (SE400-Z, Amscope) with a camera (MD500, Amscope) recorded microphotographs of hatching process every 5 minutes. A continuous LED light (1W, Amscope) was used due to light's effect on hatching (2,3). The setup is shown in Figure S2(A), and the hatching chip computer-aided design (CAD) model in Supplementary Figure S2(B).

Nonconductive cysts were gold-coated, and SEM (JEOL FS-100) was utilized to examine *Artemia* cyst morphology which shows a cup-shaped structure with porous inner walls (Figure S3). This unique structure can trap NPs (4,5) that might affect hatching. Agglomeration of NPs in saltwater forms aggregates larger than initial size (details in Section 3.1). To determine if large particles cover or diffuse into the 3D porous structure, *Artemia* cysts were photographed under SEM after hatching in the presence of various PS (50 nm, 2 µm, and 10 µm) and Ag (40 and 100 nm) NP and MP sizes at 1 mg/L concentration. PS MPs (Fluoro-Max, red fluorescent, 2 µm: Cat. No. R0200, 10 µm: Cat. No. 36-3B) and 100 nm Ag NPs (Cat. No. J67099.AE) were purchased from Thermo Scientific Chemicals and used in this study without any modification. Desiccating the cysts by air drying at ambient temperature was essential before SEM imaging. The cysts were hatched in DIW instead of ASW since the latter produces large salt particles that obscure their morphology (Figure S4). DIW instead of ASW delayed the hatching process (1), but several cysts were cracked open (due to increased internal turgor pressure, discussed in section 3.2) and observed under SEM.

Different nanoparticle sizes were used to mimic saltwater nanoparticle aggregation during hatching. Energy dispersive X-ray spectrometry (EDS) (JEOL FS-100) assessed Ag NP distribution on cysts. The results are presented in Figure S4.

Text S3. Duration of different stages, and rate of oxygen consumption

The on-chip oxygen sensor monitored the dissolved oxygen concentration (DOC) of the water. Hatching *Artemia* cysts consume oxygen causing the concentration of dissolved oxygen to decrease over time. This depletion in dissolved oxygen concentration (DDOC) at one second intervals was calculated by subtracting the DOC of each second from that of the preceding second. Figure S5 illustrates DDOC vs. hatching time for *Artemia* under various NPs treatments and a blank experiment (ASW, no cysts).

The stage durations were determined by analyzing morphological changes in the cysts as observed on optical photomicrographs (which only captured a subset of the cysts involved in hatching) and DDOC. We note that morphological transformation of 60–70% of the cysts in the photomicrographs and change in the trend of DDOC were regarded as an indicator of stage termination or the onset of the subsequent stage, given that the successful completion of stages by the cysts is also dependent on the presence of various NP conditions. As a result, this data represents the collective information of all the cysts present in the hatching chip, but it was not possible to determine what proportion of cysts survive at each stage of embryonic development in our study using the current setup.

And thus, an overall rate of oxygen consumption (oROC) is calculated based on the total oxygen consumption over 24 h of hatching experiments and weight of initial dry cysts used. This is expressed as the following formula:

$$oROC = \frac{DDOC\ after\ 24\ h\ of\ experiment\ \ in\ \frac{mg}{L} \times\ volume\ of\ water\ used\ for\ hatching\ in\ L}{24\ h\ (experimental\ duration)\ \times\ weight\ of\ initial\ dry\ cysts\ in\ mg}$$ (unit: mg O_2/h/mg dry cyst wt.)

(1)

It is also important to know the rate of oxygen consumption at each stage of the hatching process. Oxygen consumption accounts for cumulative consumption by viable cysts in initial stages (hydration, differentiation, and emergence), hatched *Artemia*, and post-hatch survivors. Moreover, DDOC at any stage of hatching (difference in DOC at the beginning and end of any stage) vary with concentrations and types of NPs (discussed in section 3.3). Accordingly, average rate of oxygen consumption (aROC) is normalized by duration and hatching rate, divided into: A) aROC during any of the first three stages (pre-hatching), $aROC_{1\text{-}3}$ and B) aROC during the hatching stage (post-hatching), $aROC_4$. $aROC_{1\text{-}3}$ is normalized by product of the duration of the any of the first three stages and the hatching rate. As previously stated, the exact number of viable cysts after each stage of the hatching process could not be determined in this study and it was assumed that the proportion of viable cysts during each stage is equivalent to the rate at which cysts successfully complete hatching and produce nauplii or hatching rate. $aROC_{1\text{-}3}$ is expressed by the following formula:

$$aROC_{1-3} = \frac{DDOC\ after\ any\ of\ the\ first\ three\ stages\ in\ \frac{mg}{L}}{Duration\ of\ that\ stage\ in\ h\ \times hatching\ rate\%}$$ (unit: mg/L/h) (2)

where the hatching rate is defined as:

$$Hatching\ rate\ (HR)\ = \frac{Total\ number\ of\ nauplii}{Total\ number\ of\ cysts}\ \times 100\ (\%)$$ (3)

The methodology for determining the hatching rate is described in section 2.5.

In contrast, $aROC_4$ is normalized by hatching stage duration, hatching rate, and fraction of live *Artemia* (FLA). This is expressed by the following formula:

$$aROC_4 = \frac{DDOC\ at\ hatching\ stage\ in\ \frac{mg}{L}}{hatching\ stage\ duration\ in\ h\ \times\ hatching\ rate\%\ \times\ fraction\ of\ live\ Artemia} \quad \text{(unit: mg/L/h)} \quad (4)$$

where the fraction of live *Artemia* (FLA) is calculated according to

$$Fraction\ of\ live\ Artemia = 1 - \frac{Number\ of\ dead\ or\ motionless\ nauplii}{Number\ of\ total\ nauplii} \quad (5)$$

Text S4. Mortality and swimming speed alteration tests

After 24 h of hatching, cysts and nauplii were transferred from the hatching chip to a shallow counting chip (1.2 mm) [Figure S2(C)] via continuous ASW flow using syringe pump (100 µL/min). The shallow cysts and nauplii monolayer distribution facilitated counting without hampering movement. Micropillars at chip outlet permit water flow but prevent cysts and nauplii from escaping. The stereo optical microscope was used to image the transferred cysts and nauplii in the counting chip after 15 seconds of manual agitation. In line with previous studies (6,7), nonmotile nauplii were considered dead, and the mortality rate was calculated according to:

$$Mortality\ rate\ = \frac{Number\ of\ motionless\ nauplii}{Total\ number\ of\ nauplii} \times 100\ (\%) \quad (6)$$

We note that this term was also interchangeably used as immobilization rate in several studies (8,9).

For swimming speed, 18-20 nauplii were returned to the hatching chip using ASW backflow from the counting chip outlet, and held in the dark for 5 minutes for acclimatization, uniform distribution, and consistent speed (10,11). Afterwards, the same digital camera equipped stereo optical microscope captured a one-minute video of the swimming nauplii in light and swimming path was tracked in ImageJ. Average swimming speed (S) was calculated for nauplii in ≥10 frames. Mortality and swimming speed were measured through triplicate experiments at each NP concentration, whereas S was determined for ≥8 nauplii. Swimming speed alteration (SSA) of the nauplii was calculated using following formula (7,12):

$$Swimming\ speed\ alteration\ (SSA) = \frac{S_{control} - S_{NP\ exposed}}{S_{control}} \times 100\ (\%) \quad (7)$$

Text S5. Hatching rate (HR) estimation

Nauplii and cysts in the counting chip were euthanized using continuous flow of 30% methanol solution in ASW. Post euthanasia, cysts and nauplii were photographed (D3100, Nikon), and the number of nauplii and cysts were counted in ImageJ based on circularity (≥ 0.9 for cysts). The steps in calculating the number of cysts and nauplii in ImageJ are shown in Figure S6. We note that, for the purpose of explanation a subset of all the cysts and nauplii were shown in this image. Total nauplii count also included transferred nauplii for swimming test. Ref (1) provides further details on the image-based automatic counting method. The hatching rate was calculated according to Eq. 2, from triplicate experiments at each NP condition.

Text S6. Statistical analysis

OriginPro (version 2023b, OriginLab) was utilized for statistical analyses. All the experiments were performed in triplicates and the data are displayed as mean ± standard deviation of the

triplicates. One-way analysis of variance (ANOVA), followed by Tukey post-hoc test was utilized to determine the significance of the different treatments after checking and confirming the normality of data (including the percentage data) via both the normal quantile-quantile plot and Shapiro-Wilk normality test with 95% confidence level. Due to the existence of negative results, the Yeo-Johnson transformation was applied exclusively to the SSA data using Scikitlearn, where the optimal power parameter (λ) is estimated via maximum likelihood, prior to conducting the one-way ANOVA test. Moreover, potential associations between the various parameters examined during the hatching process and the nauplius stage of *Artemia* were investigated in this study using Pearson correlation analyses. Two separate correlation analyses were employed due to the inability to ascertain the effects of hatching in the presence of NPs on the post-hatching stage. The first analysis examined the parameters investigated up to the hatching of *Artemia*, including the duration of all stages, aROC, and hatching rate. The second analysis focused on the post-hatching stage, examining the duration of only the hatching stage, aROC at the hatching stage, mortality rate, and swimming speed alteration (≥27 NP treatment conditions considered per category, Figure S8). If $p<0.05$, the results were considered significant.

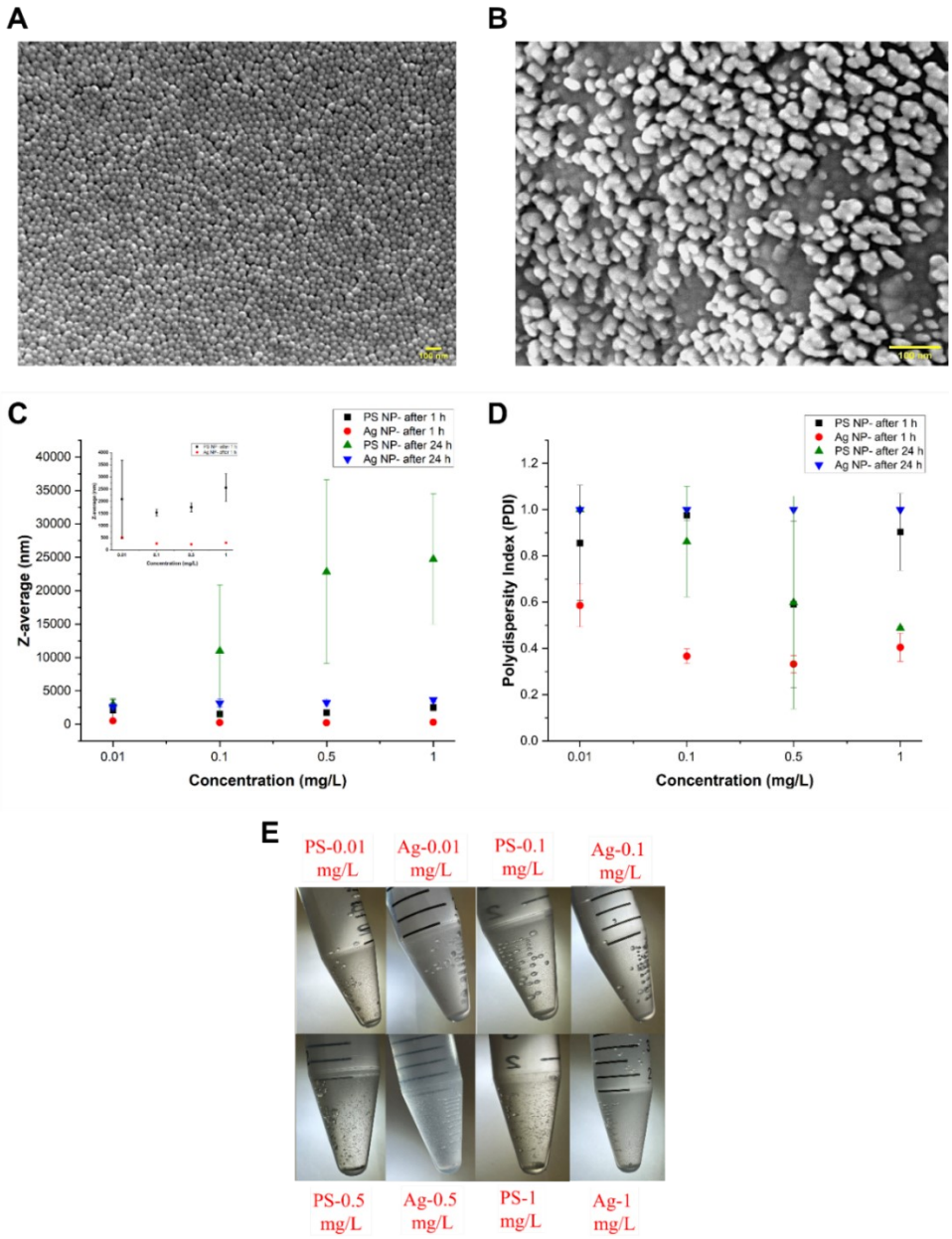

Figure S1. Morphology of the NPs and aggregation behavior at different concentrations in ASW. Morphology of -A) PS and B) Ag NPs by SEM. (C) Z-average values and (D) polydispersity index (PDI) of the NP suspension measured by DLS after 1 hour and 24 hours [inset in Figure S1(C) shows the Z-average values of NP suspension after 1 h separately]. Values are expressed as mean ± SD (triplicate or more experiments at each NP condition) (E) The photographs illustrate the

qualitative manifestation of NP aggregation and subsequent sedimentation in ASW after 24 hours at 25ºC.

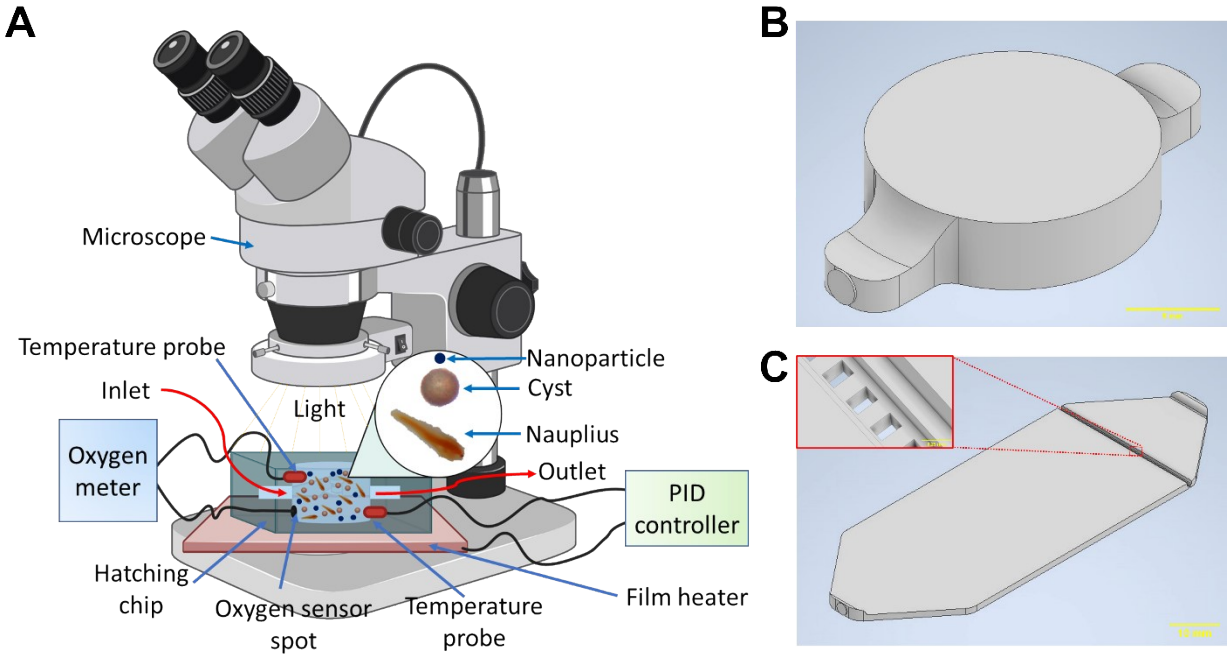

Figure S2. A) Schematic diagram of the experimental setup, B) Computer aided design (CAD) model of hatching chip (scale bar = 5 mm), and C) CAD model of counting chip (scale bar = 10 mm) [inset shows the micropillar structure to restrict escape of cysts and nauplii (scale bar = 0.25 mm)].

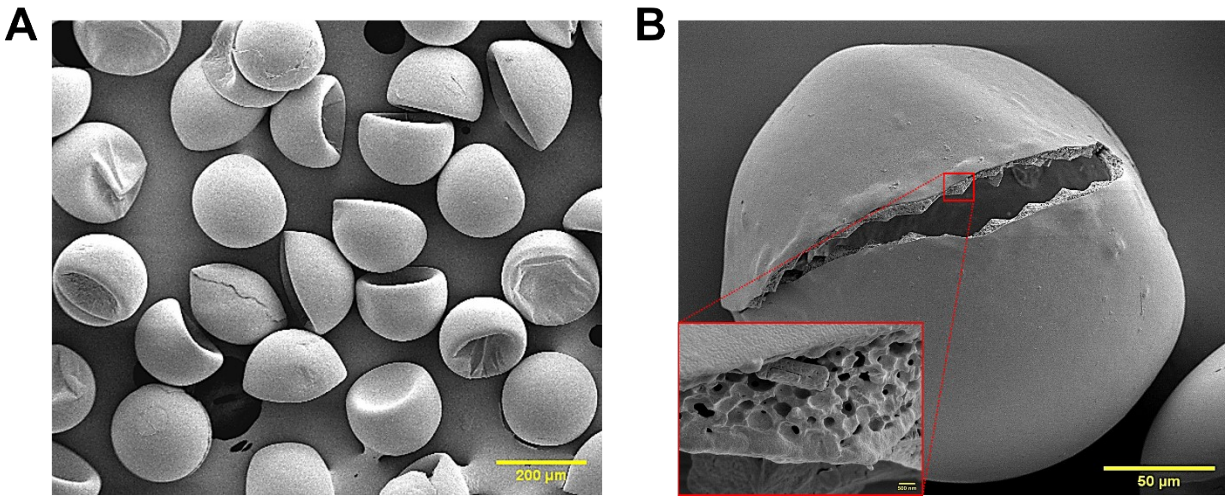

Figure S3. Scanning electron microscopy (SEM) images of- (A) *Artemia* cysts before hatching (as received) (scale bar= 200 µm). (B) Outer surface lamella and inner surface 3D porous structure (inset, scale bar= 500 nm) of as-received *Artemia* cysts (scale bar= 50 µm).

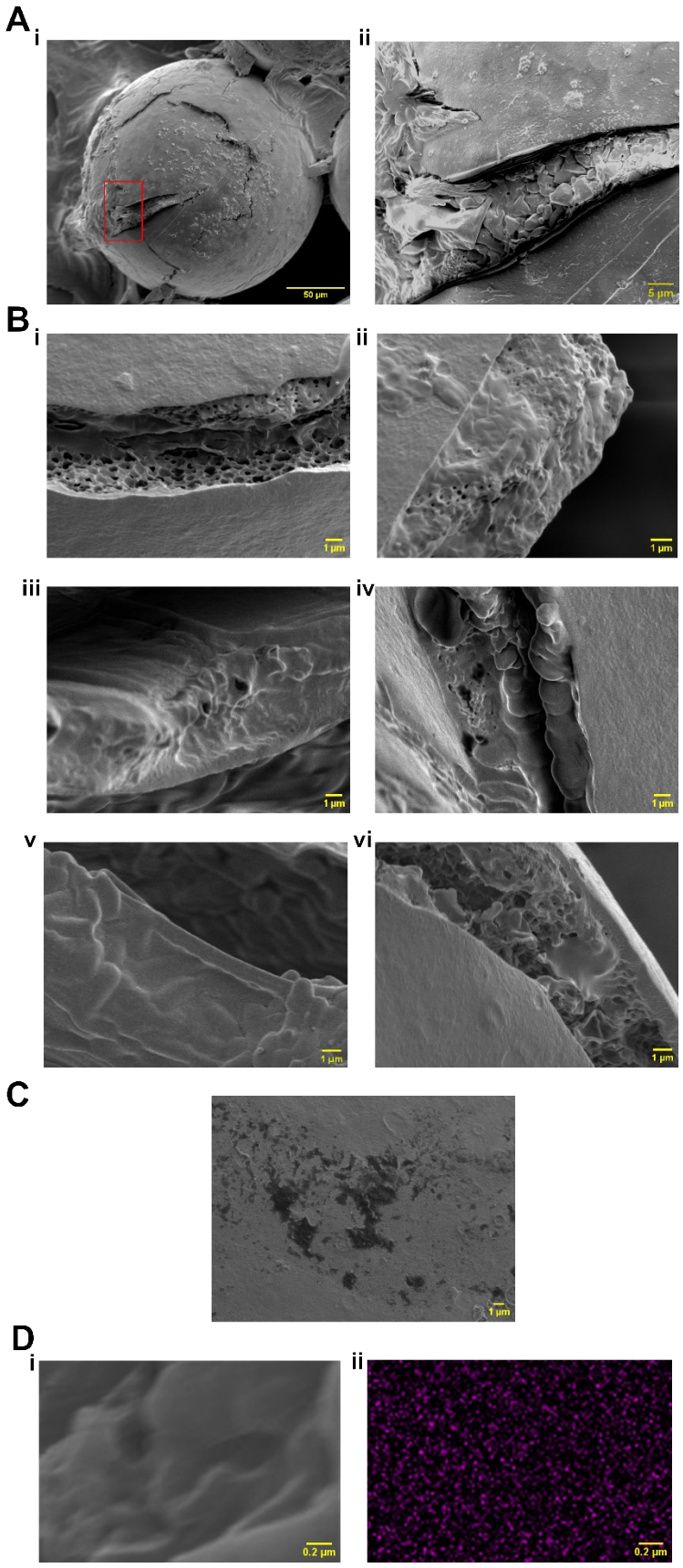
A
i
50 µm
ii
5 µm
B
i
1 µm
ii
1 µm
iii
1 µm
iv
1 µm
v
1 µm
vi
1 µm
C
1 µm
D
i
0.2 µm
ii
0.2 µm

Figure S4. Scanning electron microscopy (SEM) images and energy dispersive X-ray spectrometry (EDS) analysis of the *Artemia* cysts that hatched under various conditions. (A) SEM images of the cyst hatched in ASW reveal salt particles/crystals after water evaporation, obscuring the morphology of the cyst's inner 3D porous structure. (ii) is an enlarged view of the cyst shell fracture depicted in (i) (region marked with a red rectangle). (B) SEM images of the cyst shell fracture when the cysts were hatched in- i) only DIW, ii) 50 nm PS NPs, iii) 2 µm PS NPs, iv) 10 µm PS NPs, v) 40 nm Ag NPs, and vi)100 nm Ag NPs. (C) The SEM image reveals that larger PS NPs (10 µm) have adhered to the cyst surface (black area). (D) EDS analysis shows- i) the inner porous structure of the cyst, and ii) the distribution of 40 nm Ag NPs on the same surface as D(i) (scale bar = 0.2 µm).

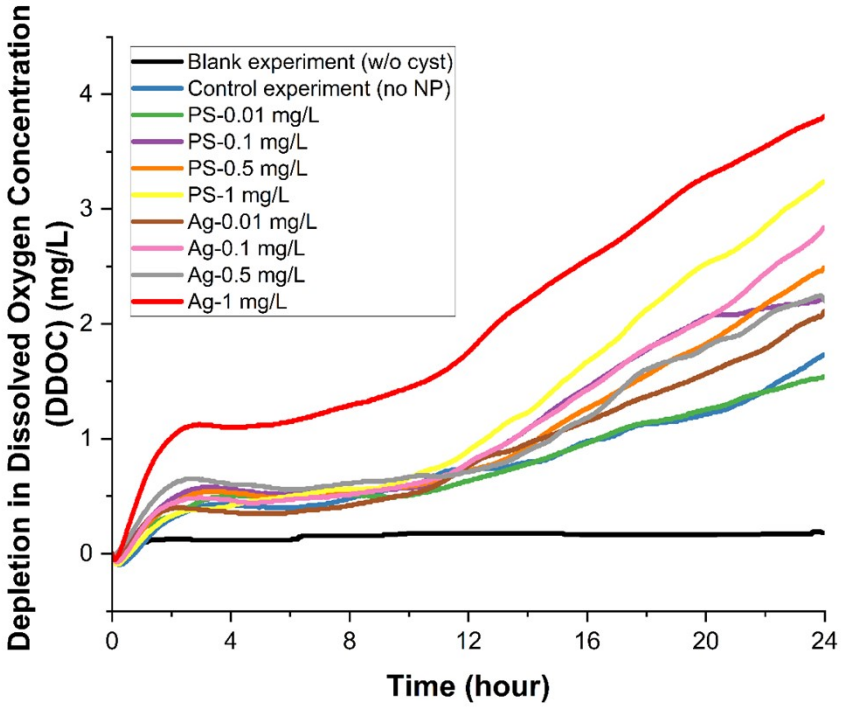

Figure S5. Average depletion of dissolved oxygen concentration (DDOC) of the hatching media with time when there were no *Artemia* cysts but only artificial saltwater (blank), *Artemia* cyst were hatched without presence of any NP (control), and *Artemia* cysts were hatched in the presence of PS and Ag NPs at various concentrations (triplicate or more experiments at each NP condition).

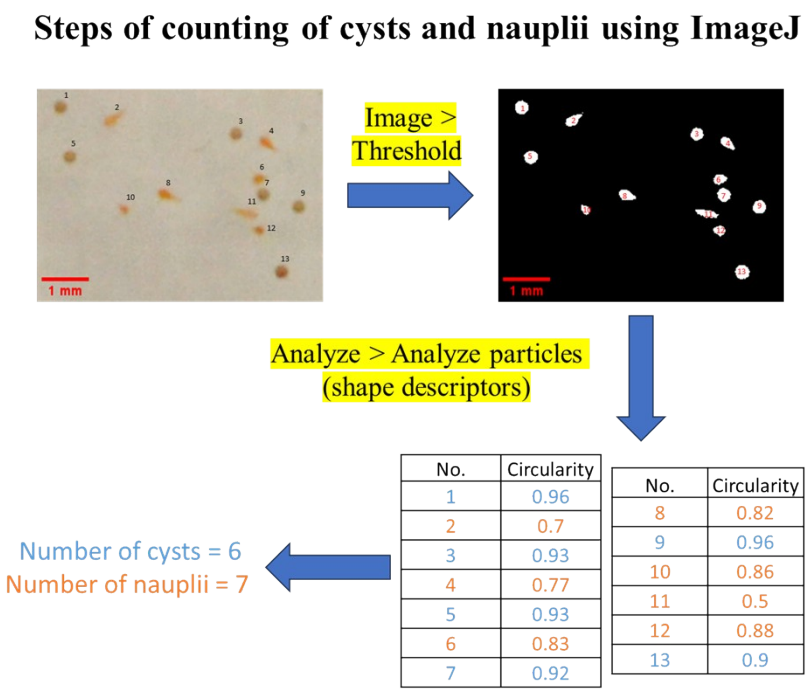

Figure S6. Steps of counting the number of cysts and nauplii using ImageJ program for the calculation of hatching rate.

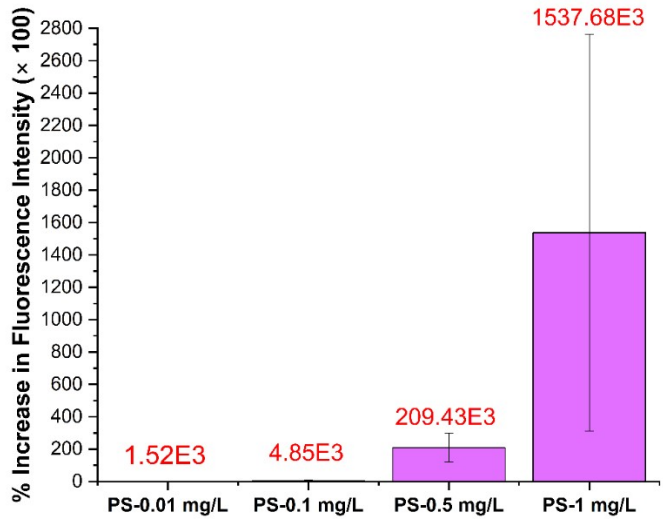

Figure S7. Percentage increase in red fluorescence intensity in *Artemia* nauplii exposed to red fluorescent PS NPs as compared to control (the numbers in red color show the average % increase in fluorescence intensity) (triplicate or more samples at each NP condition).

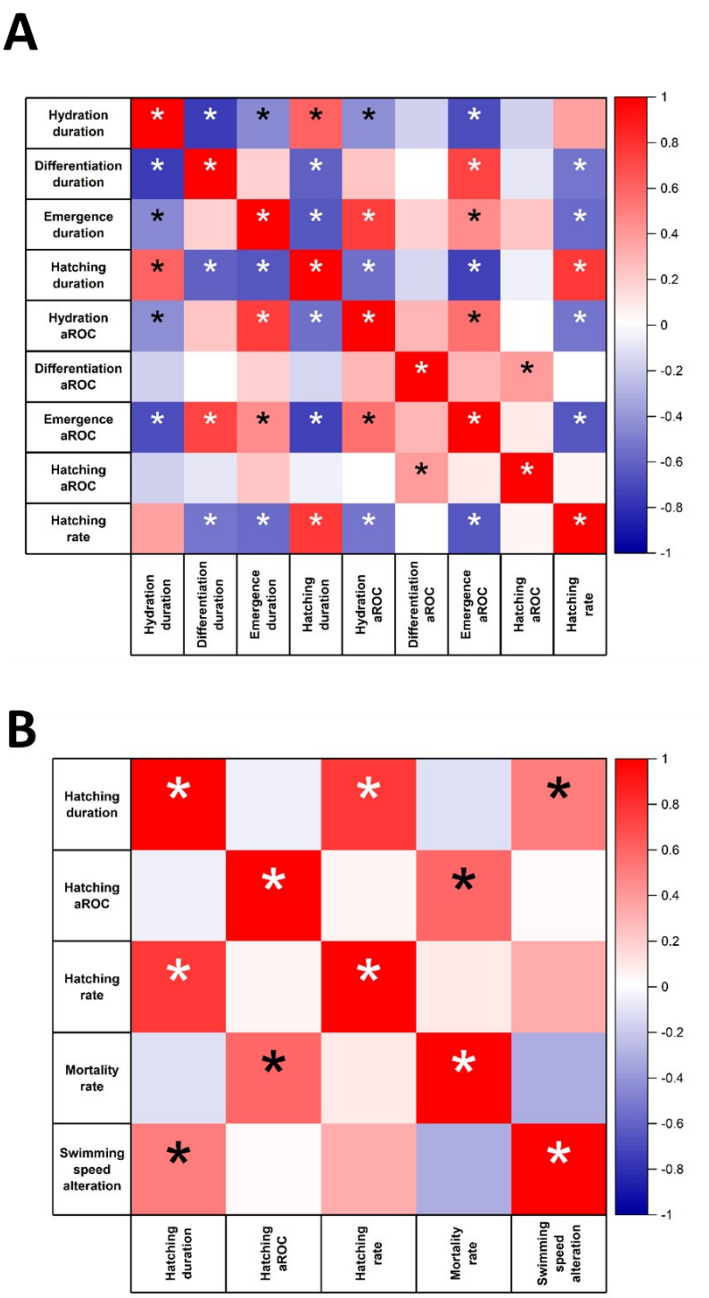

Figure S8. Pearson correlation matrix on the basis of possible association among various factors of hatching process and early stage of *Artemia* analyzed in this study irrespective of NP type and concentrations (n≥27). A) Association among different factors until hatching, and B) correlation among different factors at the final stage (hatching stage) and end-point results of mortality and swimming speed alteration. The value of Pearson correlation coefficients is shown in the adjacent color scale (-1 to 1 indicating a strong negative to strong positive association). [* represents relation is statistically significant (p<0.05)].

References

1. Dey P, Bradley TM, Boymelgreen A. The impact of selected abiotic factors on Artemia hatching process through real-time observation of oxygen changes in a microfluidic platform. Sci Rep. 2023 Apr 19;13(1):6370.

2. Kumar GR, Babu D. Effect of light, temperature and salinity on the growth of Artemia. International Journal of Engineering Science Invention. 2015;4(12):07–14.

3. Asil S, Esmaeili Fereidouni A, Ouraji H, Jani-Khalili K. The Influence of Light (Intensity and Duration) on the Cysts Hatching Parameters and Nauplii Growth of Artemia urmiana (Günther 1890). 2023 Jan 9;

4. Song Y, Song X, Sun Q, Wang S, Jiao T, Peng Q, et al. Efficient and sustainable phosphate removal from water by small-sized Al(OH)3 nanocrystals confined in discarded Artemia Cyst-shell: Ultrahigh sorption capacity and rapid sequestration. Science of The Total Environment. 2022 Jan 10;803:150087.

5. Zhao X, Song Y, Zhao Z, Gao W, Peng Q, Zhang Q. Efficient fluoride removal from water by amino Acid-enriched Artemia Cyst motivated Sub-10 nm La(OH)3 confined inside superporous skeleton. Separation and Purification Technology. 2022 Jan 15;283:120205.

6. Pecoraro R, Scalisi EM, Messina G, Fragalà G, Ignoto S, Salvaggio A, et al. Artemia salina: A microcrustacean to assess engineered nanoparticles toxicity. Microscopy Research and Technique. 2021;84(3):531–6.

7. Gambardella C, Mesarič T, Milivojević T, Sepčić K, Gallus L, Carbone S, et al. Effects of selected metal oxide nanoparticles on Artemia salina larvae: evaluation of mortality and behavioural and biochemical responses. Environ Monit Assess. 2014 Jul 1;186(7):4249–59.

8. An HJ, Sarkheil M, Park HS, Yu IJ, Johari SA. Comparative toxicity of silver nanoparticles (AgNPs) and silver nanowires (AgNWs) on saltwater microcrustacean, Artemia salina. Comparative Biochemistry and Physiology Part C: Toxicology & Pharmacology. 2019 Apr 1;218:62–9.

9. Machado AJT, Mataribu B, Serrão C, da Silva Silvestre L, Farias DF, Bergami E, et al. Single and combined toxicity of amino-functionalized polystyrene nanoparticles with potassium dichromate and copper sulfate on brine shrimp Artemia franciscana larvae. Environ Sci Pollut Res. 2021 Sep 1;28(33):45317–34.

10. Wang C, Jia H, Zhu L, Zhang H, Wang Y. Toxicity of α-Fe2O3 nanoparticles to Artemia salina cysts and three stages of larvae. Science of The Total Environment. 2017 Nov 15;598:847–55.

11. Zhu S, Xue MY, Luo F, Chen WC, Zhu B, Wang GX. Developmental toxicity of Fe3O4 nanoparticles on cysts and three larval stages of Artemia salina. Environmental pollution. 2017;230:683–91.

12. Garaventa F, Gambardella C, Di Fino A, Pittore M, Faimali M. Swimming speed alteration of Artemia sp. and Brachionus plicatilis as a sub-lethal behavioural end-point for ecotoxicological surveys. Ecotoxicology. 2010 Mar 1;19(3):512–9.